Coordinated Control of TCSC and SVC for System Damping Enhancement

Ping Lam So, Yun Chung Chu, and Tao Yu

Abstract: This paper proposes a combination of the Thyristor Controlled Series Capacitor (TCSC) and Static Var Compensator (SVC) installation for enhancing the damping performance of a power system. The developed scheme employs a damping controller which coordinates measurement signals with control signals to control the TCSC and SVC. The coordinated control method is based on the application of projective controls. Controller performance over a range of operating conditions is investigated through simulation studies on a single-machine infinite-bus power system. The linear analysis and nonlinear simulation results show that the proposed controller can significantly improve the damping performance of the power system and hence, increase its power transfer capabilities. In this paper, a current injection model of TCSC is developed and incorporated in the transmission system model. By using equivalent injected currents at terminal buses to simulate a TCSC no modification of the bus admittance matrix is required at each iteration.

Keywords: Coordinated control, damping enhancement, SVC, TCSC.

1. INTRODUCTION

A problem of interest in the power industry is the mitigation of power system oscillations. These oscillations are related to the dynamics of system power transfer and often exhibit poor damping. With utilities increasing power exchanges over a fixed network, the use of new and existing equipment in the transmission system for damping these oscillations is being considered [1]. The Thyristor Controlled Series Capacitor (TCSC) and Static Var Compensator (SVC) are both members of the Flexible AC Transmission System (FACTS) family. The TCSC is a series compensation device. With the firing control of the thyristors, it can change its apparent reactance smoothly and rapidly. This characteristic meets the demands of the modern power system that must operate flexibly and react quickly. The SVC is a shunt compensation device. It is originally designed for voltage support in power systems. Much as the TCSC, the SVC is also capable of rapid and flexible adjustment. Individually, the TCSC and the SVC can improve the damping performance of the power system. They can be combined together for superior benefits. Nevertheless, the coordination between them is very important. Otherwise, unnecessary complication may arise from their dynamic interaction affecting the performance of the power system [2].

In this paper, a control scheme using projective controls is developed for the simultaneous coordination of TCSC and SVC to enhance the damping performance of a power system. The method presented here demonstrates the control action of the TCSC in conjunction with the control action of the SVC to increase system damping and power transfer capabilities beyond those achievable with a single device. It also illustrates how the measurement and control signals are coordinated to form an effective controller. Controller performance over a range of operating conditions is investigated using linear analysis and nonlinear time domain simulations. The simulation results in a single-machine infinite-bus (SMIB) power system show that the proposed controller with coordinated control of TCSC and SVC can significantly improve system damping performance. A SMIB power system is used for simulation studies because it qualitatively represents the behavior of a multimachine system and is extremely useful in describing the general concepts of power system stability.

2. TCSC CURRENT INJECTION MODEL AND CONTROL

In this section, a current injection model is derived for the TCSC device. The installation of TCSC device

Manuscript received September 16, 2004; accepted December 2, 2004. Recommended by Guest Editor Youyi Wang.

Ping Lam So, Yun Chung Chu, and Tao Yu are with Centre for Advanced Power Electronics, School of Electrical and Electronic Engineering, Nanyang Technological University, Nanyang Avenue, Singapore 639798 (e-mails: eplso@ntu.edu.sg, eycchu@ntu.edu.sg, taoyu@ntu.edu.sg).

changes the system bus admittance matrix Y_{bus} to an unsymmetrical matrix. When the TCSC is used for time domain simulations, the modification of Y_{bus} is required at each iteration. This method has the disadvantage that a constant factorized Y_{bus} cannot be repeatedly used when the TCSC reactance is changeable in the process of transient stability calculation. For this reason, a current injection model of TCSC is developed to avoid using the modification of Y_{bus} at each iteration. The current injection model, which can be used for small signal stability and transient stability studies, is obtained by replacing the voltage across the TCSC with the current source. By using equivalent injected currents at terminal buses to simulate a TCSC no modification of Y_{bus} is required at each iteration. This method has the advantages of fast computational speed and low computer storage compared with that of modifying Y_{bus} method. In addition, the model can easily be incorporated in a dynamic simulation program, Power System Toolbox [3]. This model is also helpful for understanding the effect of the TCSC on system damping enhancement.

A TCSC connected between nodes i and j in series with a line reactance jX_l is shown in Fig. 1 and its equivalent circuit is represented in Fig. 2. In this study, the TCSC is treated as a variable capacitance. In Figs. 1 and 2, $\bar{I}_i$ and $\bar{I}_j$ are the complex currents at nodes i and j, $V_i\angle\theta_i$ and $V_j\angle\theta_j$ are the complex voltages at nodes i and j, and $\bar{V}_c$ represents a voltage across the TCSC.

From Figs. 1 and 2, it can be shown that

$$\bar{I}_j = \frac{\bar{V}_j - \bar{V}_i}{j(X_l - X_c)}, \tag{1}$$

$$\bar{V}_c = -j\bar{I}_j X_c. \tag{2}$$

The injection model is obtained by replacing the voltage $\bar{V}_c$ by a current source $\bar{I}_{js}$ in parallel with the line as shown in Fig. 3. Thus, the current injection model of TCSC as (3) and (4) is shown in Fig. 4.

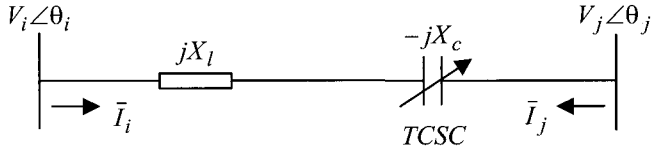

Fig. 1. Representation of a TCSC.

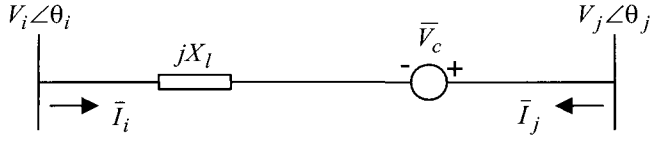

Fig. 2. TCSC equivalent circuit.

$$\bar{I}_{js} = \frac{\bar{V}_c}{jX_l} = -\frac{\bar{V}_j - \bar{V}_i}{j(X_l - X_c)}\frac{X_c}{X_l} = j\frac{K_c}{X_l(1-K_c)}(\bar{V}_j - \bar{V}_i), \tag{3}$$

$$\bar{I}_{is} = -\bar{I}_{js} = -j\frac{K_c}{X_l(1-K_c)}(\bar{V}_j - \bar{V}_i), \tag{4}$$

where $K_c = X_c/X_l$ is the compensation level of the TCSC, which refers to the line in which the TCSC is installed. (3) and (4) are used to simulate the current injection model of TCSC for time domain simulation.

For small signal stability studies, the injection currents $\bar{I}_{is}$ and $\bar{I}_{js}$, and the nodal voltages $\bar{V}_i$ and $\bar{V}_j$ corresponding to the TCSC injection model are expressed in the network d-q reference frame to couple with other components through the network as

$$\bar{I}_{is} = I_{iD} + jI_{iQ}, \tag{5}$$

$$\bar{I}_{js} = I_{jD} + jI_{jQ}, \tag{6}$$

$$\bar{V}_i = V_{iD} + jV_{iQ}, \tag{7}$$

$$\bar{V}_j = V_{jD} + jV_{jQ}. \tag{8}$$

Substituting (5) through (8) into (3) and (4), the algebraic equation (9) through (12) of the TCSC current injection model are obtained as

$$I_{iD} = \frac{K_c}{X_l(1-K_c)}(-V_{iQ} + V_{jQ}), \tag{9}$$

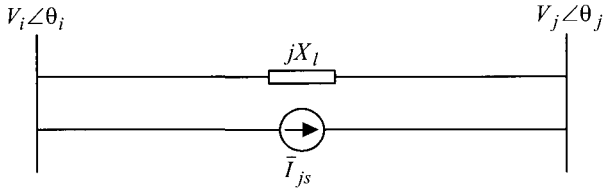

Fig. 3. Replacement of a voltage across the TCSC by a current source.

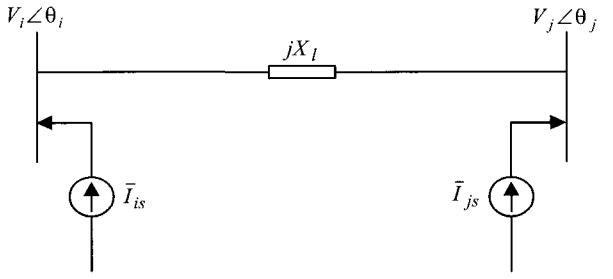

Fig. 4. Current injection model for a series compensated TCSC.

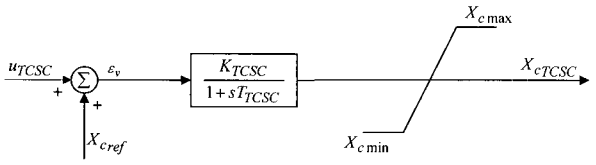

Fig. 5. TCSC control model.

$$I_{iQ} = \frac{K_c}{X_l(1-K_c)}(V_{iD} - V_{jD}), \tag{10}$$

$$I_{jD} = \frac{K_c}{X_l(1-K_c)}(V_{iQ} - V_{jQ}), \tag{11}$$

$$I_{jQ} = \frac{K_c}{X_l(1-K_c)}(-V_{iD} + V_{jD}). \tag{12}$$

The most significant feature of the TCSC is its variable degree of compensation and quick response to changing conditions, which can be used in damping out power system oscillations. Fig. 5 shows a block diagram of a TCSC control model for typical transient and oscillatory stability studies. The model includes an input signal u_{TCSC} and a reference signal X_{cref} which is the initial value of the TCSC. These inputs are summed to produce an error signal ε_v, which is fed into a first-order lag. The lag is associated with the firing control and natural response of the TCSC and is represented by a single time constant T_{TCSC}. The output of the lag block X_{cTCSC} has windup limits associated with it. These limits are based on the TCSC reactance capability. The ultimate reactance value is used to modify the line impedance of the series-compensated branch during the calculation of the network solution. A detailed description of TCSC control model is given in [4].

3. SVC CURRENT INJECTION MODEL AND CONTROL

A SVC connected at node j is shown in Fig. 6 and its current injection model is represented in Fig. 7. In this study, the SVC is treated as a variable capacitance. In Figs. 6 and 7, $\bar{I}_{jsvc}$ is the complex SVC injected current at node j, $V_i\angle\theta_i$ and $V_j\angle\theta_j$ are the complex voltages at nodes i and j.

From Figs. 6 and 7, it can be shown that

$$\bar{I}_{jsvc} = -j\bar{V}_j B_{svc}. \tag{13}$$

(13) is used for the calculation of time domain solution.

For small signal stability studies, the SVC injection current $\bar{I}_{jsvc}$ and the nodal voltage $\bar{V}_j$ corresponding

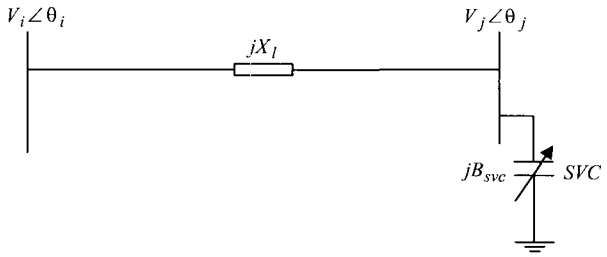

Fig. 6. Representation of a SVC.

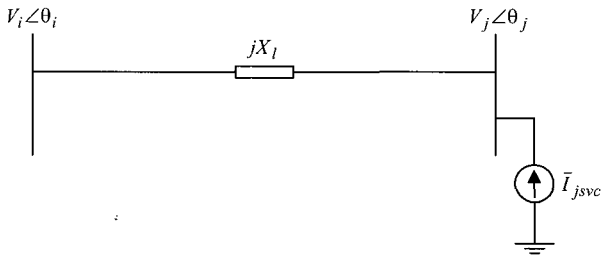

Fig. 7. Current injection model for a shunt compensated SVC.

to the SVC injection model are expressed in the network d-q reference frame to couple with other components through the network as

$$\bar{I}_{jsvc} = I_{jsvcD} + jI_{jsvcQ}, \tag{14}$$

$$\bar{V}_j = V_{jD} + jV_{jQ}. \tag{15}$$

Substituting (14) and (15) into (13), the algebraic equations (16) and (17) of the SVC current injection model are obtained as

$$I_{jsvcD} = B_{svc}V_{jQ}, \tag{16}$$

$$I_{jsvcQ} = -B_{svc}V_{jD}. \tag{17}$$

Fig. 8 shows a block diagram of a SVC control model for typical transient and oscillatory stability studies. The model includes a control signal u_{SVC} and a reference signal B_{ref} which is the initial value of the SVC. These inputs are summed to produce an error signal ε_v, which is fed into a first-order lag. The lag is associated with the firing control and natural response of the SVC and is represented by a single time constant T_{SVC}. The output of the regulator B_{SVC} is the desired susceptance of the controllable portion of the SVC and has windup limits associated with it. These limits are based on the SVC susceptance capability. The ultimate susceptance value is used to modify the susceptance of the shunt-compensated branch during the calculation of the network solution. A detailed description of the SVC control model is given in [5].

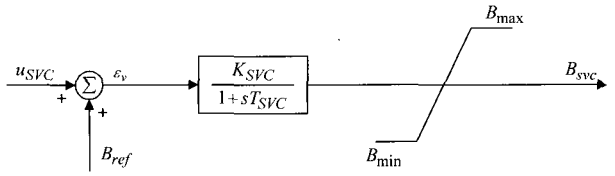

Fig. 8. SVC control model.

4. CONTROLLER DESIGN

Consider a linear system described by the state-space model

$$\dot{x} = Ax + Bu, \tag{18}$$

$$y = Cx, \tag{19}$$

where x is a state vector of length n, u is an input vector of length m, and y is an output vector of length r, and A, B and C are the state, input and output matrices, respectively. A popular approach to design a controller for this system is to formulate it as a linear quadratic regulation problem, which adopts a state feedback $u = -Kx$ such that the following cost function is minimized

$$J = \frac{1}{2}\int_0^\infty (x^T Qx + u^T Ru)dt, \tag{20}$$

where Q, R are positive definite weighting matrices to be chosen by the designer so as to achieve a certain trade-off between the closed-loop performance and the control effort. Such a control gain K can be obtained from the positive definite solution M to the Algebraic Riccati Equation

$$A^T M + MA - MBR^{-1}B^T M + Q = 0, \tag{21}$$

$$K = R^{-1}B^T M, \tag{22}$$

$$u = -Kx. \tag{23}$$

This linear quadratic approach, though optimal and mathematically elegant, is impractical for complex physical systems because usually not all state variables are measurable. For instance, a typical power system can consist of tens of state variables. It is desirable that the controller will only need to measure a few of them. In other words, an output feedback controller based on y is preferred to a state feedback controller based on x.

One way to extend the linear quadratic control to output feedback is to design an observer, which mimics the dynamics of the plant and hence estimates the state x based on the measurement y. This estimate will then be used in the state feedback control law. However, this approach will result in an unnecessarily high-order controller, which is also undesirable.

For the damping control problem studied in this paper, we adopt an alternative approach called projective controls [6-9]. This approach provides us a constant output feedback controller $u = -Ky$, which avoids the measurement of the full state vector and the complexity of a high-order dynamic controller. The approach can be briefly described as follows. Consider the closed-loop A matrix of the linear quadratic regulation problem

$$F = A - BR^{-1}B^T M. \tag{24}$$

Since the dimension of the output vector y is r, we pick r eigenvalues and eigenvectors of F and form a matrix X_r such that its columns are those chosen eigenvectors. Define the projection matrix

$$P = X_r(CX_r)^{-1}C. \tag{25}$$

and the projective control

$$u = -R^{-1}B^T MPx. \tag{26}$$

Then the control law (26) can be implemented in terms of the output y

$$u = -Ky, \tag{27}$$

where $K = R^{-1}B^T MX_r(CX_r)^{-1}$.

It was shown in [6] that the closed-loop A matrix obtained by this constant output feedback control law (27) will have the same r eigenvalues and eigenvectors as those picked from F. In this way, those r modes obtained from the linear quadratic control design (22), (23) will be preserved.

To maintain the simplicity of the coordinated controller in this paper, only two measurement signals and two control signals are used for the damping control, i.e., $r = m = 2$. Thus, the controller has the form

$$\begin{bmatrix} u_{TCSC} \\ u_{SVC} \end{bmatrix} = \begin{bmatrix} K_{11} & K_{12} \\ K_{21} & K_{22} \end{bmatrix} \begin{bmatrix} y_1 \\ y_2 \end{bmatrix} \tag{28}$$

where the matrix K coordinates the control signals u_{TCSC} and u_{SVC} (input signals into the TCSC and SVC) with the measurement signals y_1 and y_2 (see Fig. 9). In practical considerations, as the FACTS devices are mainly located in the transmission line,

the candidate measurements are restricted to network variables in the area of TCSC and SVC locations. Therefore, the selected measurement signals, y_1 and y_2, are the real power flow deviation through the line containing the TCSC ΔP_{1-3}, and the voltage magnitude deviation at the SVC location bus ΔV_3, respectively (see Fig. 10).

The complete damping controller developed here is shown in Fig. 9. The controller also includes a washout block serving as a high-pass filter, with the time constant T_w high enough to allow signals associated with oscillations to pass unchanged, and a simple filter with a time constant T_f to eliminate interactions at higher frequencies [2]. The parameters of the controller are given in the Appendix.

5. SYSTEM MODEL

To test the effectiveness of the proposed coordinated FACTS controller, a simplified model of power system is considered. The system consists of a single generator connected to a large system through two transmission lines as shown in Fig. 10. The generator is described by a subtransient fifth-order model equipped with the IEEE type ST3 exciter. The locations of TCSC and SVC are indicated in the figure. The effects of the transmission line series resistance and shunt capacitance are ignored. The system is operating with the generator delivering a real power of 0.9 p.u. to the large system. The details of the system data are given in the Appendix. The equivalent circuit of the system is shown in Fig. 11, where the FACTS devices are modeled as injected currents at terminal buses. Fig. 12 shows the phasor diagram of the system. It can be seen from Fig. 12 that by adjusting the reactance X_c of the TCSC and the susceptance B_{svc} of the SVC under the control of coordinated controller (i.e., from (3), (4) and (13), the corresponding injected currents at terminal buses will be adjusted), the system bus voltage magnitudes and phase angles can be modulated by the FACTS device regulation.

Based on the system, a state-space model is derived. A state transformation is applied to bring the C matrix into the form $[I_{rxr} \quad 0]$ first, and then the method described in the Section 4 of Controller Design is employed to design the projective controller. The Q matrix and the R matrix in (20) are chosen as $100I_{nxn}$ and I_{mxm}, respectively. Finally, the following gain matrix K of the damping controller is obtained

$$K = \begin{bmatrix} -59.5026 & 40.1890 \\ -5.3470 & -0.1034 \end{bmatrix}.$$

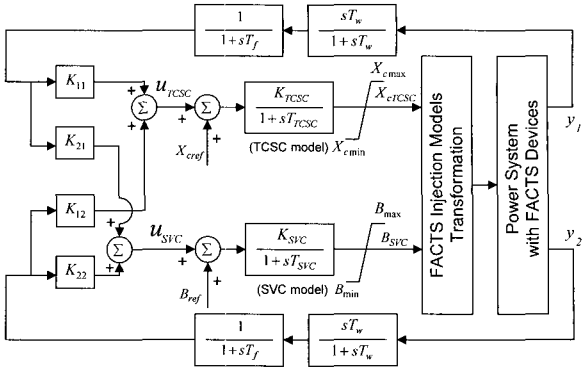

Fig. 9. Damping controller.

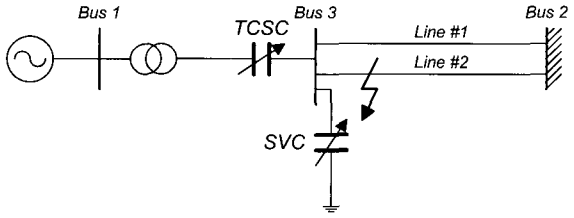

Fig. 10. A single-machine infinite-bus system with TCSC and SVC.

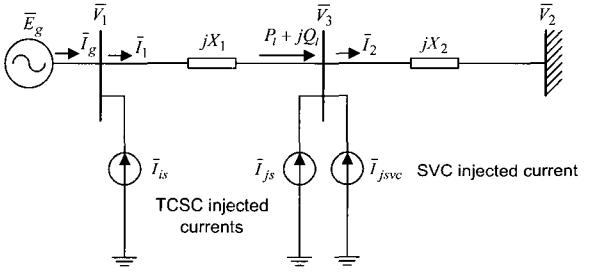

Fig. 11. The equivalent circuit of the system with TCSC and SVC.

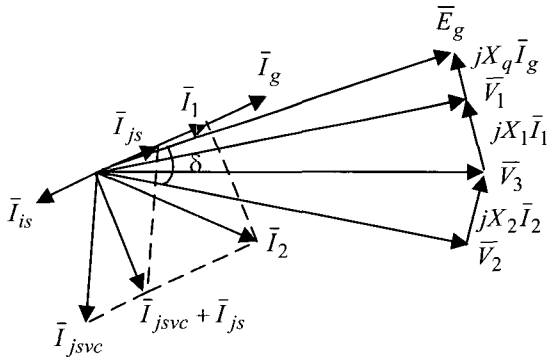

Fig. 12. Phasor diagram of the system with TCSC and SVC.

6. SIMULATION RESULTS

6.1. Linear analysis

Based on this system condition, the linearized state-space model was formed and the eigenvalues of the

system with and without the coordinated FACTS controller were computed for two different loading conditions.

Test Case 1: P=0.9 p.u.

As can be seen from Table 1, a local mode of $-0.37 \pm j11.30$ was found with a frequency of 11.30 rad/s (1.7985 Hz) and a damping ratio of 0.0327 in the system, which is weakly damped and critical. It was therefore decided to install a coordinated FACTS controller to improve the damping performance of the system. It can be seen from Table 1 that with a coordinated FACTS controller installed in the system, the damping of the local mode is greatly improved without reducing the damping of the other modes. The improved local mode has a damping ratio of 0.4589, indicating that the system is well damped under small disturbances. The results obtained are compared in Fig. 13. Fig. 13 shows that the closed-loop system shifts the weakly damped local mode of the open-loop system to the desired location without significantly changing the frequency.

Test Case 2: P = 1.1 p.u.

In order to further demonstrate the effectiveness of the proposed controller, the level of power transfer is increased from 0.9 p.u. to 1.1 p.u. The local mode with and without the coordinated FACTS controller is given in Table 2. From the results, it is seen that without a coordinated FACTS controller, the local mode has a damping ratio of 0.0027 which is almost unstable. However, when a coordinated FACTS controller is installed in the system, the damping of the local mode is increased, thereby allowing the system to operate at a higher power transfer level. The results obtained are compared in Fig. 14. It can be seen from Fig. 14 that the local mode is shifted from open loop to closed loop with added damping to the system, while the frequency shows no significant change. It is also found that the coordinated controller has little effect on the other modes.

Table 1. Effect of coordinated FACTS controller on the local mode (P=0.9 p.u.).

	Eigenvalue	Damping Ratio	Frequency (Hz)
Without FACTS	$-0.37 \pm j11.30$	0.0327	1.7985
With FACTS	$-6.24 \pm j12.08$	0.4589	1.9226

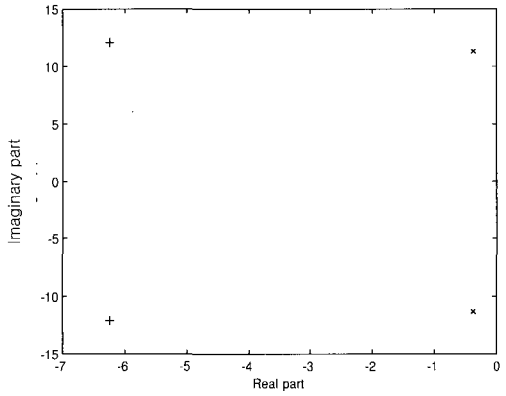

Fig. 13. Comparison of the local mode damping (P=0.9 p.u.).
x without FACTS
+ with coordinated FACTS controller

6.2. Nonlinear time domain simulations

To verify the results of linear analysis and to evaluate the performance of the designed controller, nonlinear time domain simulations of the system with and without the coordinated FACTS controller were performed for two types of disturbance:

(a) Small disturbance - switching off a transmission line was applied at 0.1s on line #2 of the system (Fig. 10).
(b) Large disturbance - a three-phase fault was applied at 0.1s on line #2 near bus 3 for 0.1s followed by the permanent tripping of the line (Fig. 10).

The performance evaluation of the coordinated FACTS controller is based on the system responses to the small and large disturbances over a range of system loading conditions. In Test Case 1, the power transfer is P=0.9 p.u., and in Test Case 2, the power transfer is increased to P=1.1 p.u.

Table 2. Effect of coordinated FACTS controller on the local mode (P=1.1 p.u.).

	Eigenvalue	Damping Ratio	Frequency (Hz)
Without FACTS	$-0.03 \pm j11.14$	0.0027	1.7730
With FACTS	$-4.01 \pm j11.99$	0.3172	1.9083

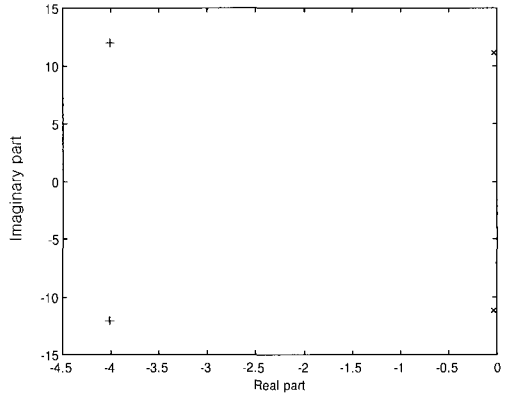

Fig. 14. Comparison of the local mode damping (P=1.1 p.u.).
x without FACTS
+ with coordinated FACTS controller

6.2.1 Small disturbance analysis

Test Case 1: P = 0.9 p.u.

Fig. 15 through Fig. 18 show the simulation results for the case with the coordinated FACTS controller compared with the case without the coordinated FACTS controller when a small disturbance as mentioned above was applied to the system. Fig. 15 through Fig. 18 show the dynamic responses of the machine rotor angle, machine speed, machine active power output and bus voltage to the small disturbance, respectively. The simulation results indicate that without a coordinated FACTS controller, the system damping is poor and the system exhibits highly oscillatory response. However, it can be observed from these figures that the coordinated FACTS controller can damp out the local mode of oscillation and the settling time is around 4 s. These simulation results correspond well with those of the linear analysis shown in Table 1. Figs. 19 and 20 show the responses of TCSC output X_c and SVC output B_{svc} to the small disturbance, respectively. As can be seen from these figures, X_c and B_{svc} vary in response to the power variations of line #1. X_c goes to zero after 4 s, while B_{svc} returns gradually to its initial value after 4 s. Initially, the SVC has to keep on injecting reactive power to maintain the bus 3 voltage at the desired value.

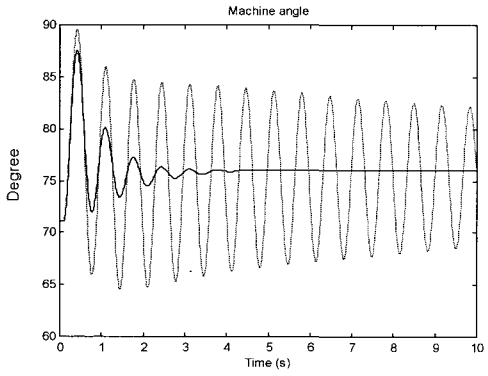

Fig. 15. Machine angle.
— with coordinated FACTS controller
-- without FACTS

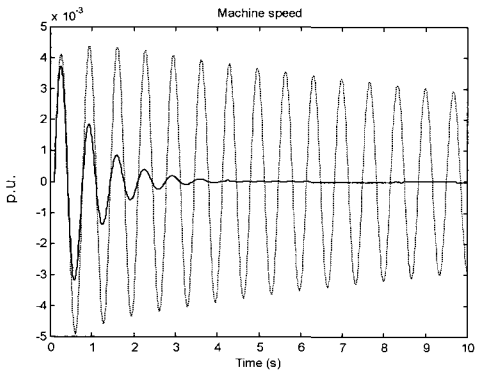

Fig. 16. Machine speed.
— with coordinated FACTS controller
-- without FACTS

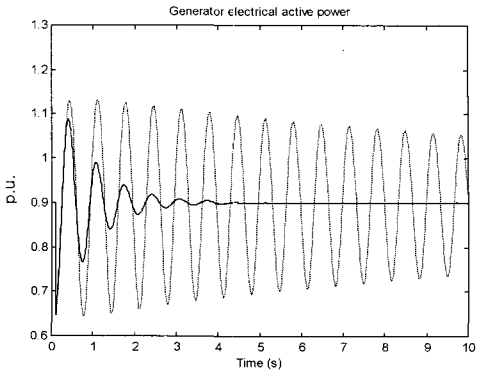

Fig. 17. Machine active power output.
— with coordinated FACTS controller
-- without FACTS

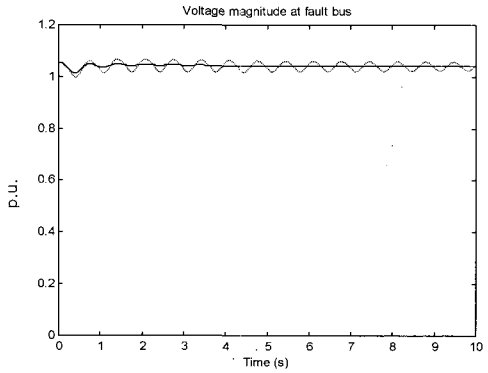

Fig. 18. Voltage magnitude at bus 3.
— with coordinated FACTS controller
-- without FACTS

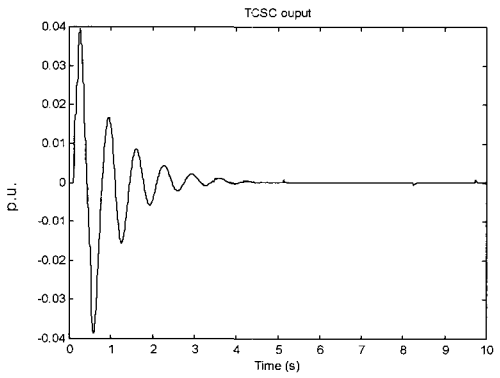

Fig. 19. TCSC output.

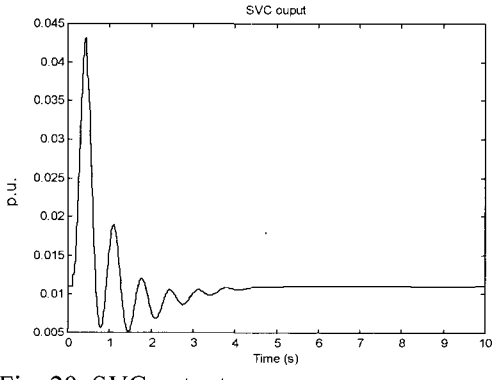

Fig. 20. SVC output.

Test Case 2: P = 1.1 p.u.

In this study, the power transfer is increased from 0.9 p.u. to 1.1 p.u. through increasing active power output of the generator. Fig. 21 through Fig. 24 show the dynamic responses of the machine rotor angle, machine speed, machine active power output and bus voltage to a small disturbance of line switching, respectively. It can be observed from the dynamic responses in these figures that with no coordinated FACTS controller in the system, the local mode is unstable with the oscillations increasing in magnitude with time. When the coordinated FACTS controller is applied to the system, the local mode oscillations are well damped and settle at a shorter time of around 3 s. All these findings again correspond well with the linear analysis results shown in Table 2. Figs. 25 and 26 show the responses of TCSC output X_c and SVC output B_{svc} to the small disturbance, respectively. Comparisons of Fig. 25 to Fig. 19 and Fig. 26 to Fig. 20 reveal that the control actions of TCSC and SVC are much stronger in Test Case 2 than those in Test Case 1. This means that the control action of the coordinated FACTS controller has a greater effect on damping the local mode of oscillation under the increased loading condition.

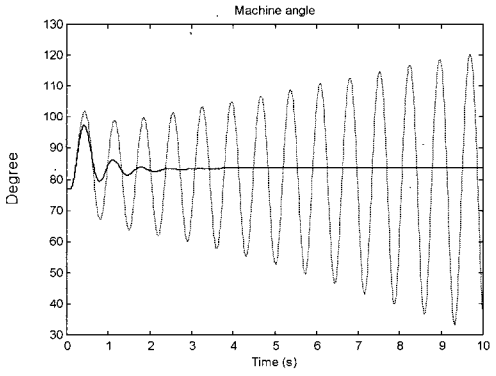

Fig. 21. Machine angle.
— with coordinated FACTS controller
-- without FACTS

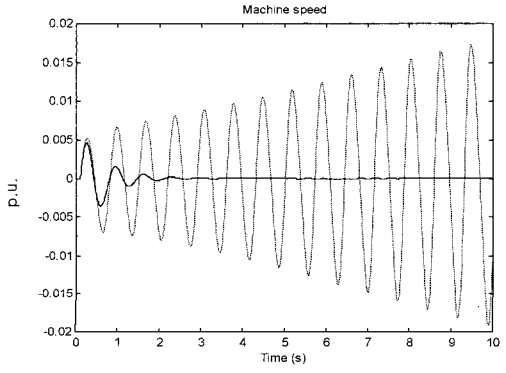

Fig. 22. Machine speed.
— with coordinated FACTS controller
-- without FACTS

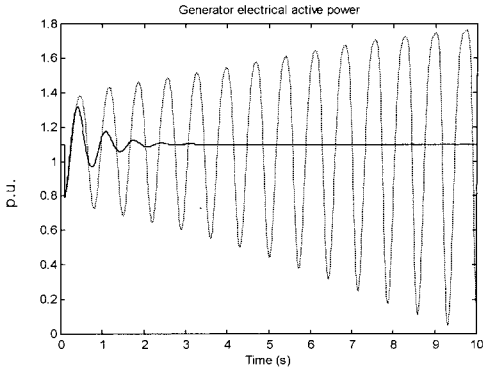

Fig. 23. Machine active power output.
— with coordinated FACTS controller
-- without FACTS

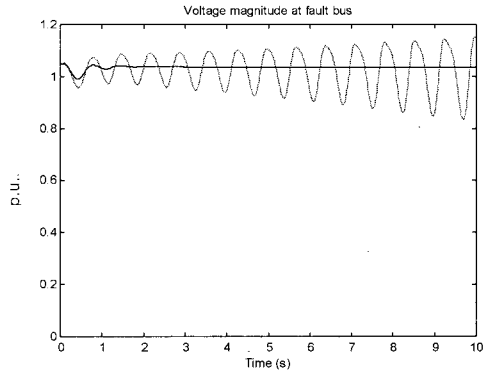

Fig. 24. Voltage magnitude at bus 3.
— with coordinated FACTS controller
-- without FACTS

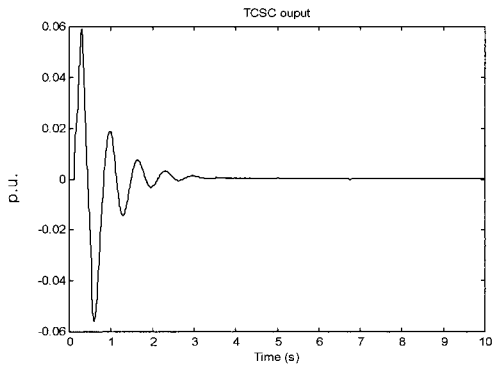

Fig. 25. TCSC Output.

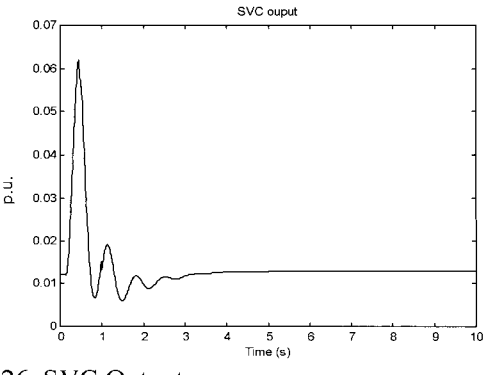

Fig. 26. SVC Output.

6.2.2 Large disturbance analysis

Test Case 1: P = 0.9 p.u.

Fig. 27 through Fig. 30 summarize the simulation results for the case with the coordinated FACTS controller compared with the case without the coordinated FACTS controller when a large disturbance as mentioned above was applied to the system. Fig. 27 through Fig. 30 show the responses of the machine rotor angle, machine speed, machine active power output and bus voltage to the large disturbance, respectively. The simulation results indicate that without a coordinated FACTS controller, the system exhibits poorly damped local oscillations following a three-phase fault. However, it is observed from these figures that the coordinated FACTS controller can significantly increase the damping of the local mode and the post-fault oscillations almost settle at 5 s. These simulation results correlate well with those of the previous linear analysis shown in Table 1. Figs. 31 and 32 show the responses of TCSC output X_c and SVC output B_{svc} to the large disturbance, respectively. It can be seen from these two figures that in order to provide additional damping to the local mode of oscillation following a large disturbance, the outputs of TCSC and SVC reach the upper and lower limits during the fault

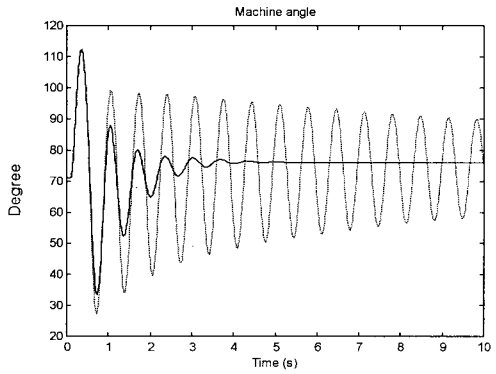

Fig. 27. Machine angle.
— with coordinated FACTS controller
-- without FACTS

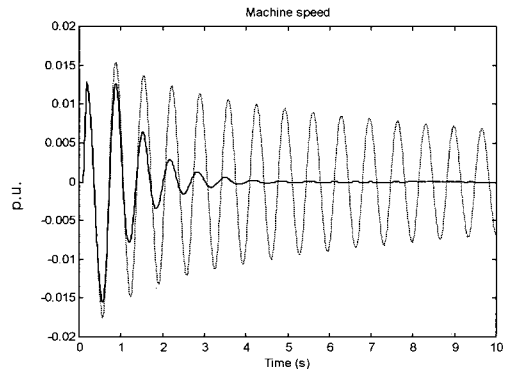

Fig. 28. Machine speed.
— with coordinated FACTS controller
-- without FACTS

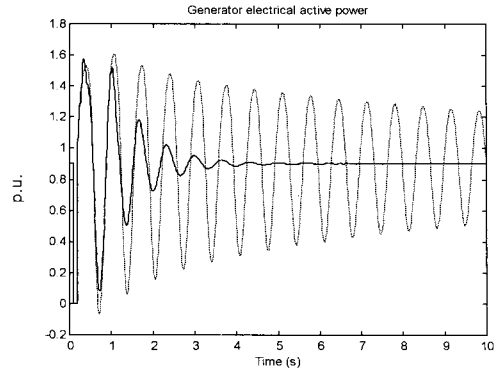

Fig. 29. Machine active power output.
— with coordinated FACTS controller
-- without FACTS

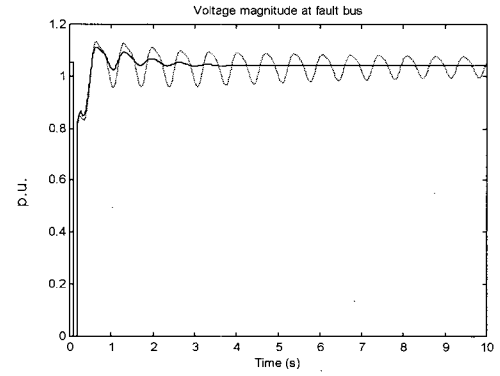

Fig. 30. Voltage magnitude at bus 3.
— with coordinated FACTS controller
-- without FACTS

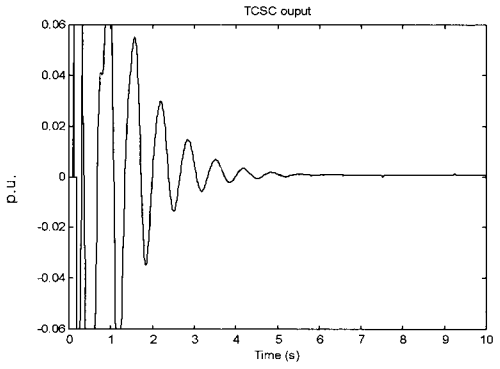

Fig. 31. TCSC output.

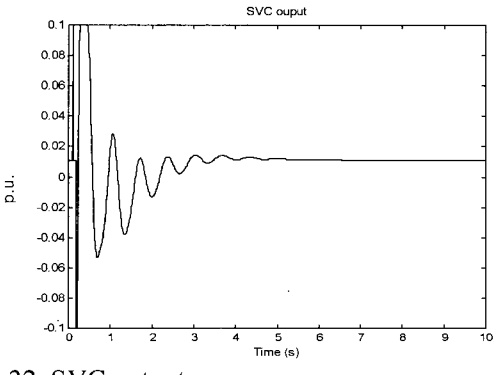

Fig. 32. SVC output.

and subsequent power swing period. These responses show different from those observed in small disturbance analysis as indicated in Figs. 19 and 20.

Test Case 2: P = 1.1 p.u.

Simulation results showing the system behavior following a large disturbance are shown in Fig. 33 through Fig. 36 when the coordinated FACTS controller is used and not used in the system. Figs. 37 and 38 show the responses of TCSC output X_c and SVC output B_{svc} to the large disturbance, respectively. It can be observed from Fig. 33 through Fig. 36 that when the power transfer is increased from 0.9 p.u. to 1.1 p.u., the coordinated FACTS controller can still provide additional damping to suppress the sustained oscillations and the settling time is around 4 s. It can be concluded that the coordinated FACTS controller can effectively damp out very large oscillations with a good effect under the increased loading condition. The damping performance of the system is improved. The coordinated control of two FACTS devices is hence satisfactory.

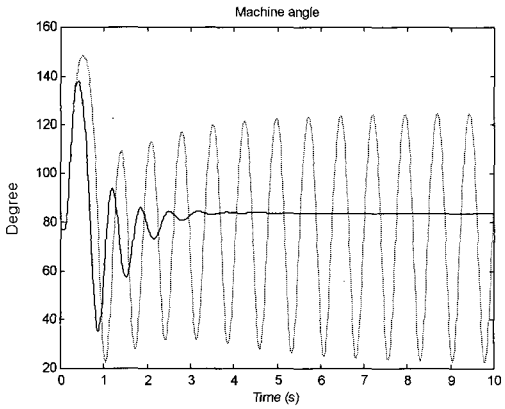

Fig. 33. Machine angle.
— with coordinated FACTS controller
-- without FACTS

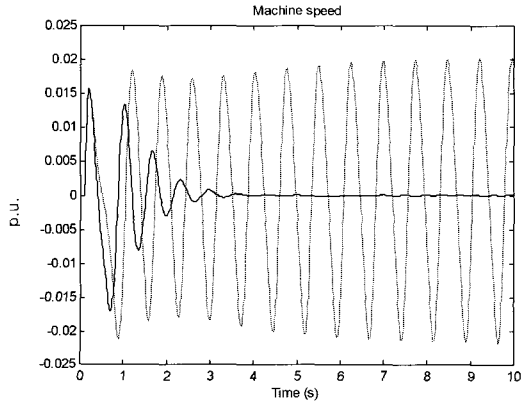

Fig. 34. Machine speed.
— with coordinated FACTS controller
-- without FACTS

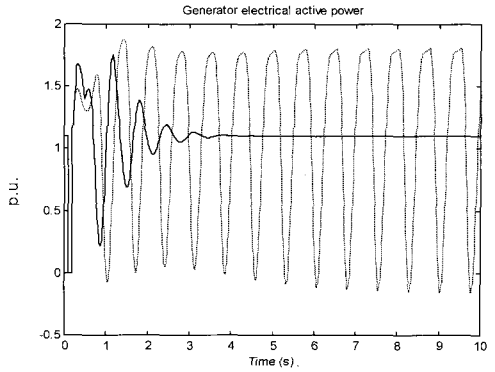

Fig. 35. Machine active power output.
— with coordinated FACTS controller
-- without FACTS

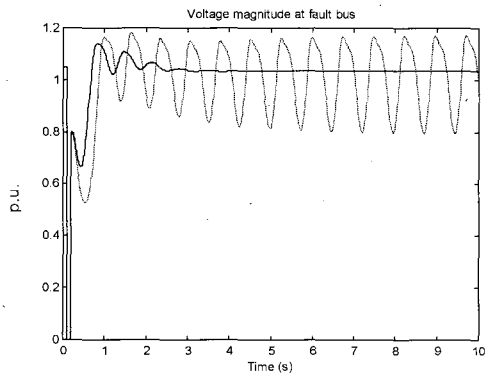

Fig. 36. Voltage magnitude at bus 3.
— with coordinated FACTS controller
-- without FACTS

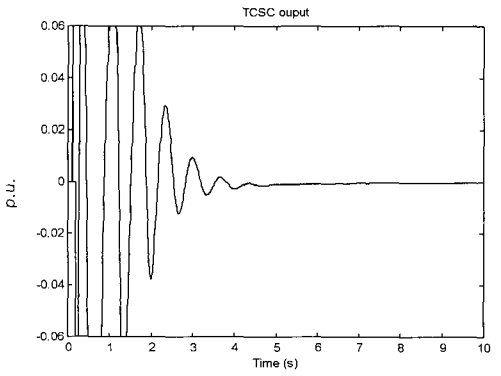

Fig. 37. TCSC output.

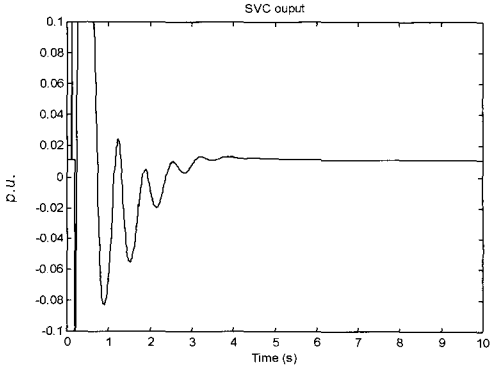

Fig. 38. SVC output.

7. CONCLUSIONS

Improvement of power system damping through coordinated control of TCSC and SVC has been investigated in a single-machine infinite-bus power system by linear analysis and nonlinear time domain simulations. An output feedback controller has been designed using projective controls. The proposed controller coordinates two measurement signals with two control signals to control the TCSC and SVC. The effectiveness of the proposed controller has been demonstrated through simulation studies over a range of operating conditions. The simulation results have shown that the proposed coordinated control scheme applied to the TCSC and SVC can effectively damp power system oscillations following small and large disturbances, thereby increasing system power transfer capabilities. To further improve the performance of the closed-loop system, the authors are presently investigating the H-infinity approach to the design of the coordinated FACTS controllers in multimachine power systems, which will result in robust controllers that can perform well under various operating conditions.

APPENDIX

System Parameters:

Synchronous generator:

$x_l = 0.15 p.u.$, $r_a = 0.0 p.u.$, $x_d = 2.0 p.u.$,
$x'_d = 0.245 p.u.$, $x''_d = 0.2 p.u.$, $T'_{d0} = 5.0 s$,
$T''_{d0} = 0.031 s$, $x_q = 1.91 p.u.$, $x'_q = 0.42 p.u.$,
$x''_q = 0.2 p.u.$, $T'_{q0} = 0.66 s$, $T''_{q0} = 0.061 s$,
$H = 2.8756 s$.

Exciter (IEEE type ST3):

$T_r = 0.0 s$, $k_A = 7.04$, $T_A = 0.4 s$, $T_B = 6.67 s$,
$T_C = 1.0 s$, $V_{R max} = 12.57 p.u.$, $V_{R min} = 0.0 p.u.$,
$V_{I max} = 0.2 p.u.$, $V_{I min} = -0.2 p.u.$, $k_J = 200$,
$k_p = 4.365$, $\beta = 20 deg.$,
$k_I = 4.83$, $x_L = 0.091 p.u.$,
$k_C = 1.096$, $E_{fd max} = 6.53 p.u.$, $k_G = 1$,
$V_{G max} = 6.53 p.u.$

Transformer:

$x_{tr} = 0.1 p.u.$

Transmission line:

$x_{23} = 0.3999 p.u.$

TCSC and SVC models:

$K_{TCSC} = 1.0$, $T_{TCSC} = 0.015 s$, $X_{c max} = 0.06 p.u.$,
$X_{c min} = -0.06 p.u.$, $K_{SVC} = 1.0$, $T_{SVC} = 0.05 s$,
$B_{max} = 0.1 p.u.$, $B_{min} = -0.1 p.u.$

Controller:

$T_f = 0.015 s$, $T_w = 5 s$.

REFERENCES

[1] J. J. Sanchez-Gasca, "Coordinated control of two FACTS devices for damping interarea oscillations," *IEEE Trans. on Power Systems,* vol 13, no. 2, pp. 428-434, May 1998.

[2] S. K. Tso, J. Liang, Q. Y. Zeng, K. L. Lo, and X. X. Zhou, "Coordination of TCSC and SVC for stability improvement of power systems," *Proc. of the IEE International Conference on Advances in Power System Control, Operation and Management,* Hong Kong, pp. 371-376, November 1997.

[3] J. H. Chow, *Cherry Tree Scientific Software: Power System Toolbox*, ver. 2.0, 1997.

[4] J. P. Paserba, N. W. Miller, E. V. Larsen, and R. J Piwko, "A thyristor controlled series compensation model for power system stability analysis," *IEEE Trans. on Power Delivery,* vol. 10, no. 3, pp.1471-1478, July 1995.

[5] E. V. Larsen and J. H. Chow, "SVC control concepts for system dynamic performance," Applications of Static Var Systems for System Dynamic Performance, *IEEE Publication 87TH0187-5-PWR,* 1987.

[6] W. E. Hopkins, J. Medanic, and W. R. Perkins, "Output feedback pole placement in the design of suboptimal linear quadratic regulators," *International Journal of Control,* vol. 34, pp. 593-612, 1981.

[7] J. Medanic and Z. Uskokovic, "Design of optimal output regulators for linear multivariable systems with constant disturbances," *International Journal of Control,* vol. 37, pp. 809-830, 1983.

[8] J. Medanic and Z. Uskokovic, "Design of decentralized static and low-order dynamic regulators for large scale systems," *Conference on Decision and Control,* San Antonio, U.S.A., December 1983.

[9] D. Arnautovic and J. Medanic, "Design of decentralized multivariable excitation controller in multimachine power systems by projective controls," *IEEE Trans. on Energy Conversion,* vol. EC-2, no. 4, pp. 598-604, 1987.

Ping Lam So joined China Light & Power Company Limited, Hong Kong, as a General Assistant Engineer in 1980 and later as Second Engineer working in the field of power system protection. He left this company in 1991 to further his studies in the U.K. He received his B.Eng. degree with first class honours in Electrical Engineering from University of Warwick in 1993, and his Ph.D. degree in Electrical Power Systems from Imperial College, University of London in 1997. He is currently an Assistant Professor in the School of Electrical and Electronic Engineering, Nanyang Technological University, Singapore. His research interests are power system dynamics, stability and control, FACTS, power quality and power line communications.

Tao Yu received his B.Eng. degree in Electrical Engineering from Shanghai Jiaotong University in 1992, P.R. China. From 1992 to 1998, he was an Engineer in China Electronics Engineering Design Institute, P.R. China. He was a research student in the School of Electrical and Electronic Engineering, Nanyang Technological University, Singapore. His research interests are power system stability and FACTS.

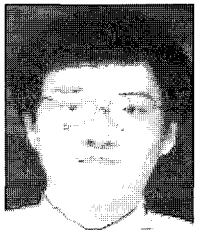

Yun Chung Chu received the B.Sc. degree in Electronics and M.Phil. degree in Information Engineering from The Chinese University of Hong Kong, Hong Kong, in 1990 and 1992 respectively, and the Ph.D. degree in Control from University of Cambridge U.K., in 1996. He worked as a Postdoctoral Fellow at The Chinese University of Hong Kong in 1996-97, a Research Associate at University of Cambridge in 1998-99, and is currently an Associate Professor in the School of Electrical and Electronic Engineering, Nanyang Technological University, Singapore. His research interests are control theory and artificial neural networks.